

Van der Waals Magnet based Spin-Valve Devices at Room Temperature

Bing Zhao¹, Roselle Ngaloy¹, Anamul Md. Hoque¹, Bogdan Karpiak¹, Dmitrii Khokhriakov¹, Saroj P. Dash^{1*}

¹Department of Microtechnology and Nanoscience, Chalmers University of Technology,

SE-41296, Göteborg, Sweden

*Corresponding author: Saroj P. Dash, Email: saroj.dash@chalmers.se

Abstract

The discovery of van der Waals (vdW) magnets opened up a new paradigm for condensed matter physics and spintronic technologies. However, the operations of active spintronic devices with vdW magnets are so far limited to cryogenic temperatures, inhibiting its broader practical applications. Here, for the first time, we demonstrate room temperature spin-valve devices using vdW itinerant ferromagnet Fe_5GeTe_2 in heterostructures with graphene. The tunnel spin polarization of the Fe_5GeTe_2 /graphene vdW interface is detected to be significantly large $\sim 45\%$ and negative at room temperature. Lateral spin-valve device design enables electrical control of spin signal and realization of basic building blocks for device application such as efficient spin injection, transport, precession, and detection functionalities. Furthermore, measurements with different magnetic orientations provide unique insights into the magnetic anisotropy of Fe_5GeTe_2 and its relation with spin polarization and dynamics in the heterostructure. These findings open opportunities for the applications of vdW magnet-based all-2D spintronic devices and integrated spin circuits at ambient temperatures.

Keywords: van der Waals magnet, room temperature, spin-valve, Fe_5GeTe_2 , graphene, spin injection, spin detection, Hanle spin precession, van der Waals heterostructures, 2D magnets, ferromagnets, 2D materials, quantum materials.

Introduction

The creation of van der Waals (vdW) heterostructures by combining two-dimensional (2D) quantum materials with complementary properties can allow the discovery of basic new physical phenomena and the development of new device concepts¹. The discovery of various 2D quantum materials and their heterostructures starting from graphene, insulators, semiconductors, superconductors, and topological materials has revolutionized both fundamental and applied research^{2,3}. The most recent addition to this 2D family are magnets, which have offered various advantages over the conventional magnets and open new perspectives in vdW heterostructure designs^{4,5}. In addition to the atomically thin and flat 2D nature of magnets, flexibility, gate tunability, strong proximity interactions, and twist angle between the layers can offer a unique degree of freedom and innovative platform for all-2D vdW devices functionalities^{4,5}.

Recently, several vdW magnets have emerged with the discovery of insulating $\text{Cr}_2\text{Ge}_2\text{Te}_6$ ⁶, semiconducting (CrI_3 ⁷, CrBr_3 ⁸), and metallic Fe_xGeTe_2 ^{9,10} nature. The insulating 2D magnets are useful for spin-filter tunneling^{8,11} and proximity-induced magnetism^{12,13}, and the metallic magnets can be used as electrodes in magnetic tunnel junctions¹⁴ and magnetic spin-orbit memory devices^{15,16} for energy-efficient and ultra-fast spintronic technologies. However, the demonstration of these device operations with vdW magnets is so far limited to cryogenic temperatures. Although room temperature magnetism and proximity effects have been recently reported using 2D magnets¹⁷⁻¹⁹, the lack of active spintronic device operation at room temperature significantly limits its practical application potential^{18,20,21}. Furthermore, a lateral spin-valve device with vdW metallic magnets is not realized yet at room temperature, an essential building block for proposed high speed and low power spin-based memory, logic, and neuromorphic computing architectures²²⁻²⁵.

Here, we demonstrate for the first time robust a room-temperature spin-valve device using metallic vdW itinerant ferromagnet Fe_5GeTe_2 in heterostructures with graphene. Significantly large spin polarization of ~45 % could be detected at room temperature due to the successful fabrication of a good vdW interface with graphene. Taking advantage of the lateral spin-valve device design, we probe the unique spin-polarized carrier injection, transport, precession, and detection functionalities with Fe_5GeTe_2 /graphene heterostructure. The spin-valve signal could be controlled by electric bias, and measurements with different magnetic orientations elucidate the evolution of magnetic anisotropy and spin polarization due to soft magnetic properties in Fe_5GeTe_2 . Such device operation advances the synergy between spintronics and 2D materials, and is expected to boost practical applications of vdW magnets in all-2D spin-based integrated circuits at room temperature.

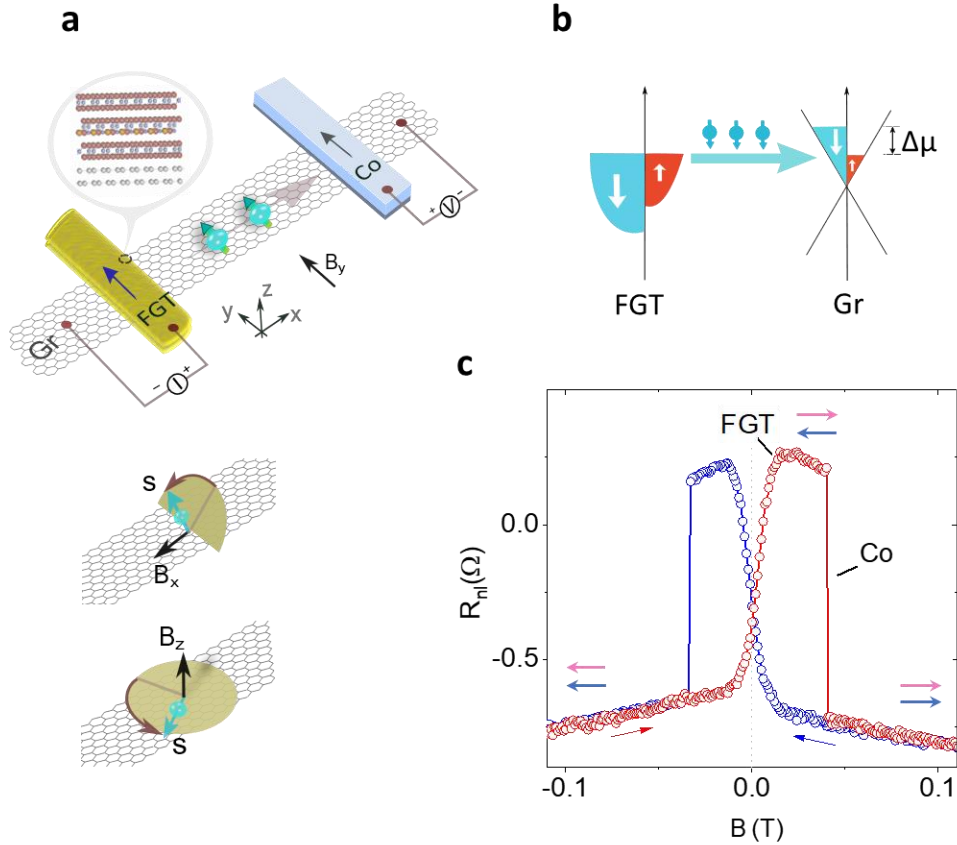


Figure 1. Room temperature spin-valve device with van der Waals magnet Fe_5GeTe_2 and graphene heterostructure. **a**, Schematic of a spin-valve device with Fe_5GeTe_2 (FGT) on a graphene (Gr) channel with reference TiO_2/Co and Ti/Au (red dots on FGT and graphene) contacts. The top inset shows the schematic of the atomic interface between FGT and graphene. The middle and bottom panels show the schematics for the Hanle spin precession measurements with B_x and B_z fields, respectively. **b**, Schematic illustration for spin injection from FGT into the graphene channel through the vdW gap, inducing a non-equilibrium spin accumulation $\Delta\mu$ in graphene. **c**, The measured nonlocal (NL) spin-valve signal $R_{nl}=V_{nl}/I_{dc}$ for parallel and antiparallel alignment of FGT and Co electrodes (light pink and blue arrows) with an applied bias current $I_{dc}=+15\ \mu A$ across the FGT/Gr junction and NL voltage V_{nl} measured by the TiO_2/Co detector, as shown in the measurement geometry in **a**. A representative spin-valve data is shown for an in-plane magnetic field sweep at an angle of -60° in the x - y plane relative to the $+y$ axis. The arrows show the sweeping direction of the magnetic field. The switching fields for FGT and Co electrodes in the spin-valve measurement are indicated. The measurements were performed in Dev 1 at room temperature.

Results and Discussion

The schematic of the spin-valve device with measurement geometry is shown in Fig. 1a, consisting of multilayer Fe_5GeTe_2 as a spin injector (source) or detector (drain) on the few-layer graphene spin transport channel. The measurements with magnetic field (B) sweep along the y -axis provide information about in-plane spin polarization of Fe_5GeTe_2 along the y -axis, whereas the Hanle spin

precession measurements with B along $x(z)$ -axis is an unambiguous and reliable approach to extract the (initial) injected spin states and its dynamic properties. The vdW gap between Fe_5GeTe_2 and graphene should allow an efficient spin injection and detection process in the heterostructure (Fig. 1b). The motivation behind the use of Fe_5GeTe_2 is its ferromagnetic order with Curie temperature (T_c) close to room temperature^{18,21}, compared to Fe_3GeTe_2 with $T_c \sim 220$ K^{9,10}. An increased saturation magnetization in Fe_5GeTe_2 can also provide larger spin polarization due to the Fe-rich vdW heterostructure forming a three-dimension (3D)-like spin-pair interaction^{20,21}. The motivation behind the use of graphene as the channel material is its excellent spin transport properties²⁶ and ideal combination with Fe_5GeTe_2 for vdW heterostructure-based spin-valve devices operating at room temperature. The Fe_5GeTe_2 /graphene heterostructures are prepared on Si/SiO₂ substrate employing exfoliation and dry transfer techniques. The nonmagnetic Ti/Au and ferromagnetic (TiO₂/Co) contacts are nanofabricated on Fe_5GeTe_2 flakes and graphene channels for reference electrodes. The contact resistance of Fe_5GeTe_2 /graphene is ~ 6 k Ω and TiO₂/Co is ~ 1 -5 k Ω . For details of the device fabrication, see the Methods section and Supplementary Fig. S1.

Room temperature spin valve with Fe_5GeTe_2 /graphene heterostructure

We first measured the spin-valve operation with spin injection from Fe_5GeTe_2 into the graphene channel at room temperature. A source current was applied between Fe_5GeTe_2 and the reference Au electrode on graphene, and the nonlocal (NL) voltage was measured between detector Co contact and another reference Au contact (Fig. 1a). Figure 1c shows the measured spin-valve signal with switchings originating from Fe_5GeTe_2 injector and Co detector contacts with different coercive fields (H_c) for an in-plane magnetic (B) field sweep. By comparing the reference spin valve signal with all-Co injector and detector contacts (see Supplementary Fig. S2a), we can confirm that the sharp switching at higher H_c in the signal is the contribution from the detector Co contact, and the slow and lower H_c switching is originating from the Fe_5GeTe_2 injector electrode. The observation of the robust spin-valve signal shows the presence of an in-plane spin component in Fe_5GeTe_2 at room temperature.

To investigate the anisotropy in spin injection from Fe_5GeTe_2 and to probe the out-of-plane spin component (along the z -axis), an angle dependence (Fig. 2a) of the spin-valve measurement was performed from $+90^\circ$ to -90° in the x - y plane (Fig. 2b and Fig. 2c). The measurements show that the Fe_5GeTe_2 has a very soft magnetization and can be easily rotated in the sample plane by a small applied field; however, it has a robust out-of-plane remnant spin polarization. Specifically, several features can be observed from in-plane angle-dependent measurements. First, the switching field of detector Co increases with the magnetic field rotation angle Φ , consistent with the strong uniaxial magnetic anisotropy of Co in a narrow stripe geometry (see Supplementary Fig. S2d and Fig. S2e). Second, the spin-valve signal can be seen as the result of the non-zero in-

plane projection of the injected spin polarization from Fe₅GeTe₂ on the magnetic moment direction of the detector Co electrode. Here, if we suppose the magnetic moment of Co remains along the y-axis in the small field range (-0.1 to 0.1 Tesla, T), we observe that the saturation field of Fe₅GeTe₂ is smallest at around $\Phi \approx -50^\circ$. These measurements show the presence of an in-plane magnetic anisotropy in the Fe₅GeTe₂ flake.

Third, the $\pm 90^\circ$ data represents the x-axis Hanle (xHanle) curves for spin precession measurement. Contrary to conventional symmetric xHanle signal with both Co-Co injector-detector devices (see Supplementary Fig. S2d), a sine-shaped signal is observed in the FGT-Co injector-detector geometry, which shows an out-of-plane spin injection S_z from Fe₅GeTe₂ into the graphene channel (Fig. 2d and Fig. 2e)^{27,28}. Notably, there is almost no symmetric Hanle component at $\Phi = \pm 90^\circ$, suggesting minimum remnant spins S_y , i.e., no remnant magnetic moment M_y along y-axis when $B_x = 0$ T. Such observation indicates the soft magnetic property of the Fe₅GeTe₂ flake with the in-plane component along the x-axis at remanence, however, with the presence of a robust out-of-plane spin component S_z . Forth, both the spin valve and the xHanle signals coexist, for example, at $\Phi = \pm 60^\circ$ and $\pm 80^\circ$. Here, the contribution of S_y projection is identical; however, the S_z spin precession direction is opposite for positive and negative angles Φ , which induces a different sign of the sine-shaped Hanle signal. To extract the sine-shaped component from the nonlocal signals, we analyzed the measured data by removing the Co switching and symmetrizing the switched curves (see Supplementary Note 1 and Fig. S3). The magnitude of the normalized signal to the one at $\Phi = 0^\circ$ as a function of Φ is presented in Fig. 2f, agreeing well with the $\cos(\Phi) \sim \Phi$ curve. It confirms the projection of in-plane magnetic moment M_{eff} in Fe₅GeTe₂ on the y-axis versus in-plane magnetic field B rotation follows the $\cos(\Phi)$ relation. From these observations of spin-valve and xHanle measurements, we found the Fe₅GeTe₂ flake to be a very soft ferromagnet with both in-plane and out-of-plane magnetic moments.

Large spin polarization in Fe₅GeTe₂/graphene interface

To calculate the spin polarization of Fe₅GeTe₂, we consider the magnitude of the spin-valve signal (for $\Phi = 0^\circ$), $\Delta R_{nl} = P_{FGT} \cdot P_{Co} \cdot \lambda_{gr} \cdot R_{sq} \cdot \exp(-L_{ch}/\lambda_{gr})/w_{gr}$, where only the spin polarization of Fe₅GeTe₂, P_{FGT} , is unknown; and the other parameters (P_{Co} the spin polarization of Co, λ_{gr} spin diffusion length, R_{sq} square resistance, L_{ch} channel length and w_{gr} width of the graphene channel) are extracted from the reference Co₁-Co₂ spin valve with the standard Hanle formula. From the standard Hanle data fitting, we extract the spin lifetime in the graphene channel $\tau_s = 198 \pm 13$ ps, spin diffusion constant $D_s = 0.008 \pm 0.001$ m²/s and spin diffusion length $\lambda_{gr} = 1.26 \mu m$. The spin polarization of Co is $P_{Co} = 10.1\% \pm 4.1\%$ (see more details in Supplementary Note 4). From the FGT-Co spin valve signal, we calculate the lower limit of effective in-plane spin polarization of Fe₅GeTe₂, $|P_{FGT}| = 35.8\% \pm 1.3\%$. To be noted, in the spin valve signal, the switching of Co occurs before full saturation of Fe₅GeTe₂ (for $\Phi = 0^\circ$), which is much larger than the Co coercive field. Therefore, a

much larger spin valve signal can be achieved if the detector Co contact is designed to have a higher coercive field, and effective $|P_{\text{FGT}}|$ can be as large as $\sim 44.9\%$ if the fully saturated Fe_5GeTe_2 is considered. The out-of-plane spin polarization along the z-axis is calculated to be $P_z = 9.5\% \pm 0.3\%$ from x-Hanle data in Fig. 2e. Moreover, the out-of-plane magnetic moment M_z seems to be robust enough in the in-plane x-Hanle measurements and total spin polarization can be calculated by $P_{\text{tot}} = \sqrt{(P_{\text{in}}^2 + P_z^2)} = \sqrt{0.449^2 + 0.095^2} = 45.9\%$ (see Supplementary Note 2 for details). Such a large spin polarization at the $\text{Fe}_5\text{GeTe}_2/\text{Gr}$ interface suggests an efficient spin injection efficiency due to the vdW gap, the sharp interface between $\text{Fe}_5\text{GeTe}_2/\text{Gr}$, and the large saturation magnetization of Fe_5GeTe_2 at room temperature.

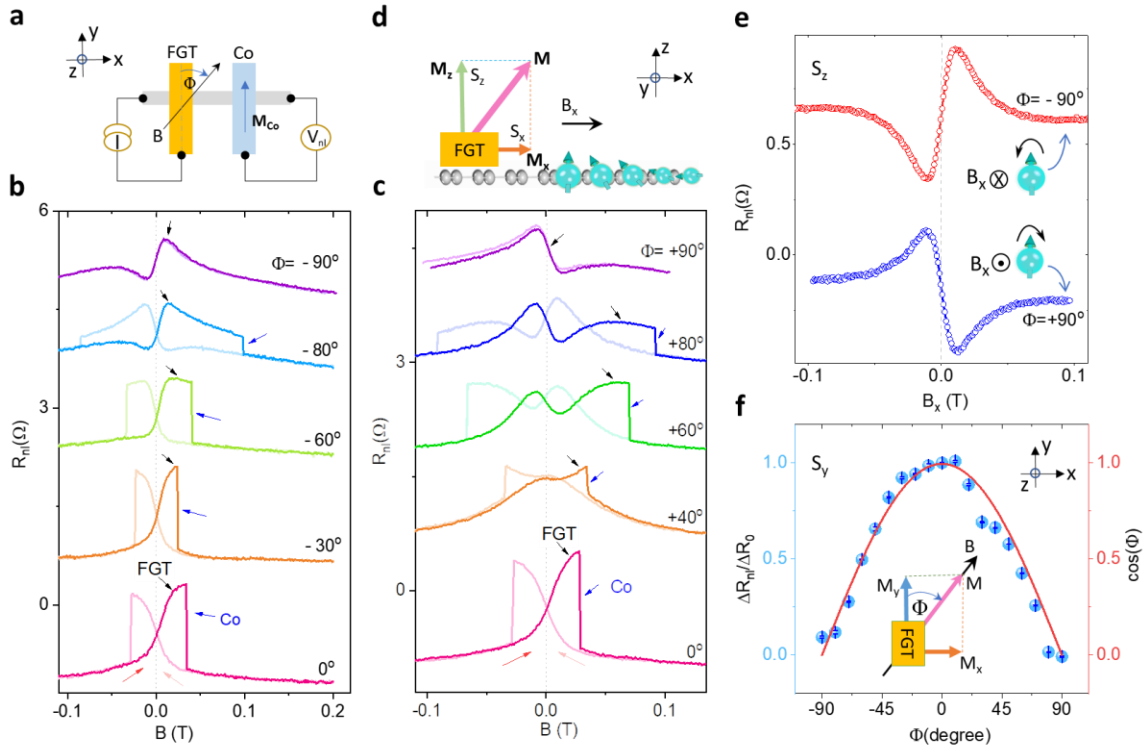


Figure 2. Anisotropy in spin-valve signal and spin precession. *a.* The top view schematic of the spin valve device with in-plane B field sweep in the x - y plane with an angle Φ with respect to y -axis. *b, c.* Angle dependence of the spin valve signal with angle $\Phi = 0$ to -90° and 0 to $+90^\circ$, respectively. The switchings of injector FGT and detector Co electrodes in the spin valve signal are shown by black and blue arrows, respectively. A y -axis shift is added in the signals for clarity, and a small hysteresis of $\sim 3.5\text{mT}$ from the magnet is corrected using control experiments of reference graphene Hanle signals. *d.* The side view schematic of the device for magnetic moment configuration in FGT with an external B_x field. M is the magnetic moment with components M_x (M_z) along the x (z)-axis. S_z and S_x are the corresponding injected spin orientations. *e.* xHanle signals at $\Phi = \pm 90^\circ$ with parabolic background subtraction. The inset shows the cartoon for spin precession direction with opposite B fields. *f.* Normalized spin valve signal components and spin precession direction.

comparison with the cosine function with the in-plane B rotation angle Φ . The error bars are within the data points, calculated based on the noise level of the signal. The inset is the schematic for the magnetic moment projection on the axes, where S_y is injected spins from M_y magnetization of FGT. The measurements were performed in Dev 1 at room temperature.

Negative spin polarization of Fe₅GeTe₂/graphene interface

To examine the sign of spin polarization of Fe₅GeTe₂ contacts on graphene, we performed detailed bias dependence measurements and compared them with the standard Co contacts. We investigated the bias current dependence of the spin injection and extraction signal from Fe₅GeTe₂ on the graphene channel (Fig. 3a), where the direction of the generated spins s are found to be dependent on the polarity of the applied current bias. Reversing the bias current direction ($+/-I_{dc}$) in Fe₅GeTe₂ results in an accumulation of opposite spin polarization in graphene and hence an inverted behavior of the measured spin-valve signal (Fig. 3b). These measurements demonstrate that spin polarization direction can be controlled by electrical spin injection and extraction in Fe₅GeTe₂. As a reference, the control experiment with the Co₁-Co₂ spin-valve was also performed with $+/-I_{dc}$ bias currents (Fig. 3c), showing the expected sign change of the signal. The magnitude of the spin-valve signals with bias current for FGT-Co₂ and Co₁-Co₂ spin valves are shown in Fig. 3d for the spin injection and extraction regimes. The accumulated spin density is observed to scale linearly with the applied bias current for both Fe₅GeTe₂ and Co contacts on the graphene channel.

Surprisingly, we notice that the sign of spin signal with one Fe₅GeTe₂ electrode is the opposite compared to that of the standard all-Co spin valves, which implies the negative or opposite spin polarization of Fe₅GeTe₂ compared to Co contacts (see Supplementary Note 3). For example, in Fig. 3e, we plotted the comparison of spin valve signals with FGT-Co₂ and Co₁-Co₂ injector-detector contact configurations for positive bias currents, showing opposite spin polarization between Co and Fe₅GeTe₂ contacts. Such a negative spin polarization is found to be robust and could be reproducibly observed in multiple devices (also see data from Dev 2 and Dev 3 in Supplementary Fig. S5a and Fig. S5b). A possible origin can be due to the unique band structure with the 'down' spin state as the majority in Fe₅GeTe₂ at the interface with graphene. These observations agree with a recent theoretical prediction²⁹, where the Fe atoms, with d-orbital electrons, dominate the contribution of the unique asymmetry in the electron population between spin-up and spin-down states.

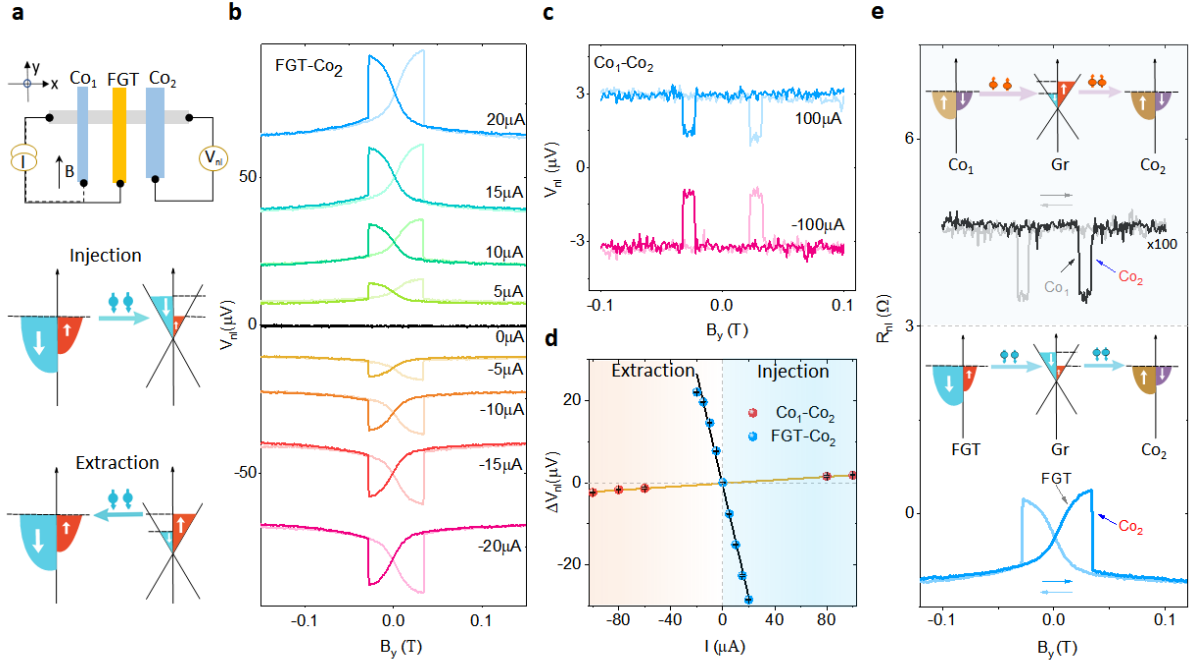


Figure 3. Negative spin polarization of $\text{Fe}_5\text{GeTe}_2/\text{graphene}$ interface. *a.* Top panel: Schematic of the nonlocal measurement geometries for FGT- Co_2 and Co_1 - Co_2 spin valves. Bottom panels: Schematics for the spin injection and extraction process with FGT, showing the accumulation of down and up spins in the graphene channel, respectively. *b.* Spin valve signals with FGT- Co_2 for different bias currents of $\pm I_{dc}$. *c.* Co_1 - Co_2 Spin valve signals with $I_{dc} = \pm 100 \mu\text{A}$. *d.* Bias dependence of the spin valve signal magnitude and the linear fittings. The error bars (within the data points) are calculated from the standard deviation of the measured background noise in the data. *e.* Comparison of spin valve signals ΔR_{nl} ($= \Delta V_{nl}/I$) with Co_1 - Co_2 and FGT- Co_2 injector-detector contact configurations, showing opposite spin polarization between Co and FGT contacts. The Co_1 - Co_2 spin valve signal is multiplied by 100 along the y-axis for clarity. The inset in the top and bottom panels are the schematics of the spin injection and detection process by Co_1 and FGT, respectively. Both nonlocal spin valves share the same detector Co_2 with the same switching field in the signals. All the measurements were performed on Dev 1 at room temperature.

Out of plane spin precession and dynamics in $\text{Fe}_5\text{GeTe}_2/\text{graphene}$ spin valve

Next, to investigate Hanle spin precession of in-plane spin polarization, we carried out the measurements with an out-of-plane magnetic field (B_z) sweep³⁰. However, with a soft magnet Fe_5GeTe_2 as an injector, the magnetic moment M and the injected spin s rotate to the out-of-plane direction with a small external B_z field (Fig. 4a). The magnetic moment M also has an in-plane component M_{eff} which induces the spin polarization S_{xy} , corresponding to the components along the y - and x -axis (S_y and S_x). As shown in Fig. 4b, we observed a modified Hanle signal due to the combined effect of magnetic moment rotation of Fe_5GeTe_2 and precession of the injected

spins in the graphene channel. Furthermore, measurements with the different magnetization direction of Fe₅GeTe₂ and Co electrodes result in the sign reversal of Hanle curves ($\pm M_{eff}$), as shown in Fig. 4c (bottom panel). To eliminate the non-spin-related background from the measured data, we take an average of the signals R_{avg} and decompose them into symmetric (Sys) and antisymmetric (Ays) components (Fig. 4c, top and middle panels), corresponding to the spin components S_y and S_x respectively.

First, considering the symmetric signal for the entirely out-of-plane moment of Fe₅GeTe₂ for $|B_z| > 0.15$ T, there is no contribution to the spin precession signal and the magnitude of R_{nl} should be null. Notably, we observe that the symmetric signal shows a comparable magnitude of signals at $B_z = 0$ T and $|B_z| > 0.15$ T. Therefore, the in-plane spin S_y at $B_z \sim 0$ T is also negligible and so is the remanent magnetization M_y . At the intermediate stages, where B_z is in the range of 0 to ± 0.15 T, the M_y increases to a peak value and decreases again to zero for the magnetic moment M saturation along the z-axis (Fig. 4a). This is supported by our simple simulation, which shows that M_y should be minimum at $B \sim 0$ T (see Supplementary Note 4 and Note 5). Secondly, the antisymmetric component of the signal suggests the existence of the spins S_x along the x-axis. We can fit the S_x component and obtain the effective spin polarization $P_x = 15.3\% \pm 4.8\%$ (see Supplementary Fig. S4c.). These observations suggest that the in-plane magnetic moment M_{eff} does not align with the long axis of the flake, which can be due to the in-plane magnetic anisotropy and crystal symmetry of Fe₅GeTe₂. Therefore, the observed z-axis Hanle signals are combined effects of magnetic moment rotation of Fe₅GeTe₂, and precession and dephasing of the injected spins S_x and S_y in the graphene channel (see more discussions in Supplementary Note 1).

Furthermore, we extracted the magnetic moment rotation angle α_M with B_z from the z-axis Hanle curves using opposite magnetic configurations $\pm M_{eff}$ in Fig. 4c (see details in Supplementary Note 4). It shows the evolution of local magnetic moment near the Fe₅GeTe₂/graphene interface with B_z and its saturation at ~ 0.15 T (Fig. 4d). To correlate the orientation of spin injection signal to the magnetization behavior of the Fe₅GeTe₂ with the external B_z field, the anomalous Hall effect (AHE) measurement was also performed in the same Fe₅GeTe₂ flake (Fig. 4e). The AHE curve suggests a rotation of the magnetization in Fe₅GeTe₂ along the z-axis, and the saturation point of the AHE curve is also consistent with that of the $\alpha_M \sim B_z$ relation. Detailed angle dependence of the AHE measurement performed in a similar Fe₅GeTe₂ flake (see Supplementary Note 6) suggests a presence of the magnetic anisotropy in Fe₅GeTe₂ (see Supplementary Note 2). This observation agrees well with the spin-valve Hanle spin precession results.

In addition to spin injection from Fe₅GeTe₂ into the graphene channel, we also demonstrated spin detection by Fe₅GeTe₂ using Dev 2 as shown in Supplementary Note 7 and Supplementary Fig. S8. The bias dependence of the spin signals with the Fe₅GeTe₂ detector also showed good linearity in the measured bias range. Furthermore, the gate voltage dependence of the spin valve signal

for the spin injection and detection by Fe_5GeTe_2 shows a tunability (Supplementary Fig. S8c and S9c), mainly due to the modulation of the graphene channel resistance with gate voltage and conductivity mismatch between the Fe_5GeTe_2 and graphene channel³¹.

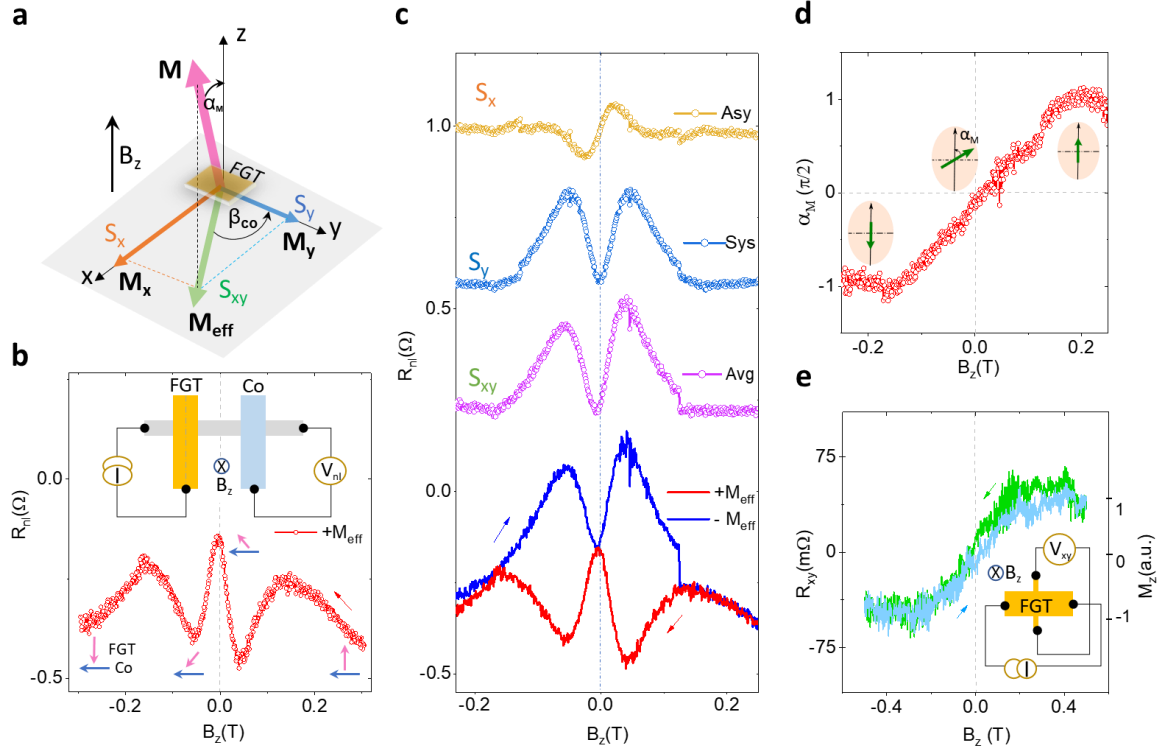


Figure 4. Out-of-plane Hanle signal in Fe_5GeTe_2 /graphene spin valve. **a.** Schematic of the magnetic moment configuration in FGT, where M represents the total magnetic moment of FGT, rotating with external out-of-plane magnetic field B_z . M_{eff} is the effective in-plane projection of M with components (M_x , M_y) along the x - and y -axis. S_{xy} is the injected in-plane spins from M_{eff} with components S_x and S_y , along the x - and y -axis, respectively. β_{co} is the relative angle between M_{eff} and the y -axis. α_M is the angle between M and the z -axis. **b.** Measured Hanle spin precession signal with B_z sweep for $I_{\text{dc}} = +15 \mu\text{A}$ with in-plane magnetization $+M_{\text{eff}}$ in FGT. The blue and green arrows show the FGT and Co magnetic moment evolution with B_z . The red arrow shows the B sweeping direction. The top inset shows the schematic of measurement geometry. **c.** Hanle curves for the parallel and antiparallel magnetization direction of injector FGT and detector Co electrodes. Symmetric (Sys) and anti-symmetric (Ays) components of the averaged Hanle signal R_{avg} , where $R_{\text{avg}} = [R_{\text{nl}}(+M_{\text{eff}}) - R_{\text{nl}}(-M_{\text{eff}})]/2$, and $R_{\text{ays}} = [R_{\text{avg}}(B) + R_{\text{avg}}(-B)]/2$; $R_{\text{sys}} = [R_{\text{avg}}(B) - R_{\text{avg}}(-B)]/2$. **d.** Relation of the extracted α_M as a function of B_z . The insets are the corresponding magnetic moment evolution in FGT with the external field B_z . **e.** Anomalous Hall effect (AHE) signal of FGT (R_{xy}) as a function of magnetic field B_z sweeps along the z -axis. The M_z on the right axis is the out-of-plane magnetic moment in an arbitrary unit, $M_z = \pm 1$ suggesting a total out-of-plane magnetic moment saturation. The inset shows the AHE measurement geometry. All the measurements were performed on Dev 1 at room temperature.

Summary and Outlook

In conclusion, we demonstrated a robust room-temperature operation of van der Waals magnet-based spin-valve devices. Highly efficient spin injection, transport, dynamics, and detection could be observed with a large negative spin polarization of $\text{Fe}_5\text{GeTe}_2 \sim 45\%$ in the heterostructure with graphene channel. Furthermore, soft ferromagnetic properties and spin polarization anisotropy in Fe_5GeTe_2 could be probed via angle dependence measurements in the spin-valve devices. These studies provide unique insights into the room-temperature magnetism of Fe_5GeTe_2 and its relation with spin transport and precession in graphene heterostructure devices. These results establish the integration of vdW magnets with graphene spin valve devices and have a vast potential in developing all-2D spintronics devices and integrated circuits at room temperature. Furthermore, this will also bring a strong synergy between 2D quantum materials and spintronics with the possibility of further control the figure of merits by twist angle between the layers, magnetic proximity effects, and gate tunability for energy-efficient and ultra-fast spintronic devices. These room-temperature developments in van der Waals heterostructure will open opportunities for the use of van der Waal magnets for fundamental studies in condensed matter physics and device applications in spintronic sensors, memory, logic, and neuromorphic computing architectures^{32,33}.

Methods

Fabrication of devices and electrical measurements

The Fe_5GeTe_2 (FGT) crystal (from Hq Graphene) flakes (20~50 nm) were exfoliated and dry transferred onto the exfoliated few-layer graphene (from HOPG) on an n^{++} -doped Si substrate with 285 nm SiO_2 . For the device fabrication, the nonmagnetic and magnetic contacts were prepared by multiple electron beam lithography (EBL) processes and electron beam evaporation of metals. The nonmagnetic Ti/Au contacts were first prepared on FGT flakes and graphene for reference electrodes. The ferromagnetic contacts (TiO_2/Co) on graphene were prepared in a two-step deposition and an oxidation process was adopted, 0.4 nm Ti was deposited, followed by a 10 Torr O_2 oxidation for 10 min each, followed by 60 nm of Co deposition. Measurements were performed at room temperature with a magnetic field up to 0.8 Tesla and a sample rotation stage in vacuum conditions. The electronic measurements were carried out using current source Keithley 6221, nanometer 2182A, and dual-channel source meter Keithley 2612B.

Acknowledgments

The authors acknowledge financial supports from EU Graphene Flagship (Core 3, No. 881603), Swedish Research Council VR project grants (No. 2016–03658), 2D TECH VINNOVA competence center (No. 2019-00068), Graphene center, EI Nano, and AoA Materials program at Chalmers University of Technology. We acknowledge the help of staff at Quantum Device Physics laboratory and Nanofabrication laboratory in our Department of Microtechnology and Nanoscience at Chalmers University of Technology.

Data availability

The data that support the findings of this study are available from the corresponding authors on a reasonable request.

Author information

Affiliations

Department of Microtechnology and Nanoscience, Chalmers University of Technology, SE-41296, Göteborg, Sweden

Bing Zhao, Roselle Ngalay, Anamul Md. Hoque, Bogdan Karpiak, Dmitrii Khokhriakov, & Saroj P. Dash

Contributions

B.Z and R.N fabricated and characterized the devices. A.M.H, B.K, D.K, S.P.D. participated in device preparation and measurements. B.Z. and S.P.D conceived the idea and designed the experiments. B.Z. and S.P.D. analyzed and interpreted the experimental data, compiled the figures, and wrote the manuscript with inputs from all co-authors. S.P.D. supervised the research project.

Corresponding author

Correspondence to Saroj P. Dash, saroj.dash@chalmers.se

Competing interests

The authors declare no competing interests.

Reference

1. Geim, A. K. & Grigorieva, I. V. Van der Waals heterostructures. *Nature* **499**, 419–425 (2013).
2. Novoselov, K. S., Mishchenko, A., Carvalho, A. & Castro Neto, A. H. 2D materials and van der Waals heterostructures. *Science* **353**, aac9439 (2016).
3. Žutić, I., Matos-Abiague, A., Scharf, B., Dery, H. & Belashchenko, K. Proximitized materials. *Mater. Today* **22**, 85–107 (2019).
4. Gibertini, M., Koperski, M., Morpurgo, A. F. & Novoselov, K. S. Magnetic 2D materials and heterostructures. *Nat. Nanotechnol.* **14**, 408–419 (2019).
5. Gong, C. & Zhang, X. Two-dimensional magnetic crystals and emergent heterostructure devices. *Science* **363**, (2019).
6. Gong, C. *et al.* Discovery of Intrinsic Ferromagnetism in Two-Dimensional van der Waals Crystals. *Nature* vol. **546** 265–269 (2017).
7. Huang, B. *et al.* Layer-dependent ferromagnetism in a van der Waals crystal down to the monolayer limit. *Nature* vol. **546** 270–273 (2017).

8. Kim, M. *et al.* Micromagnetometry of two-dimensional ferromagnets. *Nature Electronics* **2**, 457–463 (2019).
9. Fei, Z. *et al.* Two-dimensional itinerant ferromagnetism in atomically thin Fe₃GeTe₂. *Nat. Mater.* **17**, 778–782 (2018).
10. Deng, Y. *et al.* Gate-tunable room-temperature ferromagnetism in two-dimensional Fe₃GeTe₂. *Nature* **563**, 94–99 (2018).
11. Klein, D. R. *et al.* Probing magnetism in 2D van der Waals crystalline insulators via electron tunneling. *Science* **360**, 1218–1222 (2018).
12. Karpiak, B. *et al.* Magnetic proximity in a van der Waals heterostructure of magnetic insulator and graphene. *2D Mater.* **7**, 015026 (2019).
13. Ghiasi, T. S. *et al.* Electrical and thermal generation of spin currents by magnetic bilayer graphene. *Nat. Nanotechnol.* (2021) doi:10.1038/s41565-021-00887-3.
14. Wang, Z. *et al.* Tunneling Spin Valves Based on Fe₃GeTe₂/hBN/Fe₃GeTe₂ van der Waals Heterostructures. *Nano Lett.* **18**, 4303–4308 (2018).
15. Wang, X. *et al.* Current-driven magnetization switching in a van der Waals ferromagnet Fe₃GeTe₂. *Science Advances* **5**, eaaw8904 (2019).
16. Alghamdi, M. *et al.* Highly Efficient Spin-Orbit Torque and Switching of Layered Ferromagnet FeGeTe. *Nano Lett.* **19**, 4400–4405 (2019).
17. Li, Q. *et al.* Patterning-Induced Ferromagnetism of Fe₃GeTe₂ van der Waals Materials beyond Room Temperature. *Nano Letters* vol. **18** 5974–5980 (2018).
18. Zhang, H. *et al.* Itinerant ferromagnetism in van der Waals Fe_{5-x}GeTe₂ crystals above room temperature. *Physical Review B* vol. **102** 064417 (2020).
19. Wang, H. *et al.* Above Room-Temperature Ferromagnetism in Wafer-Scale Two-Dimensional van der Waals Fe₃GeTe₂ Tailored by a Topological Insulator. *ACS Nano* **14**, 10045–10053 (2020).
20. Seo, J. *et al.* Nearly room temperature ferromagnetism in a magnetic metal-rich van der Waals metal. *Sci Adv* **6**, eaay8912 (2020).
21. May, A. F. *et al.* Ferromagnetism Near Room Temperature in the Cleavable van der Waals Crystal Fe₅GeTe₂. *ACS Nano* **13**, 4436–4442 (2019).
22. Behin-Aein, B., Datta, D., Salahuddin, S. & Datta, S. Proposal for an all-spin logic device with built-in memory. *Nat. Nanotechnol.* **5**, 266–270 (2010).
23. Manipatruni, S. *et al.* Scalable energy-efficient magnetoelectric spin-orbit logic. *Nature* **565**, 35–42 (2018).
24. Grollier, J. *et al.* Neuromorphic Spintronics. *Nat Electron* **3**, (2020).
25. Zollner, K., Gmitra, M. & Fabian, J. Swapping Exchange and Spin-Orbit Coupling in 2D van der Waals Heterostructures. *Phys. Rev. Lett.* **125**, 196402 (2020).
26. Roche, S. *et al.* Graphene spintronics: the European Flagship perspective. *2D Mater.* **2**, 030202 (2015).
27. Safeer, C. K. *et al.* Room-Temperature Spin Hall Effect in Graphene/MoS₂ van der Waals Heterostructures. *Nano Lett.* **19**, 1074–1082 (2019).
28. Benítez, L. A. *et al.* Tunable room-temperature spin galvanic and spin Hall effects in van der Waals heterostructures. *Nat. Mater.* **19**, 170–175 (2020).
29. Joe, M., Yang, U. & Lee, C. First-principles study of ferromagnetic metal Fe₅GeTe₂. *Nano Materials Science* **1**, 299–303 (2019).
30. Tombros, N., Jozsa, C., Popinciuc, M., Jonkman, H. T. & van Wees, B. J. Electronic spin transport and spin precession in single graphene layers at room temperature. *Nature* **448**, 571–574 (2007).
31. Han, W. *et al.* Tunneling spin injection into single layer graphene. *Phys. Rev. Lett.* **105**, 167202 (2010).
32. Dieny, B. *et al.* Opportunities and challenges for spintronics in the microelectronics industry. *Nature Electronics* **3**, 446–459 (2020).
33. Lin, X., Yang, W., Wang, K. L. & Zhao, W. Two-dimensional spintronics for low-power electronics. *Nature Electronics* **2**, 274–283 (2019).